ACS APPLIED MATERIALS & INTERFACES

Research Article

www.acsami.org

Tailor-Made Charge-Conversional Nanocomposite for pH-Responsive Drug Delivery and Cell Imaging

Yan Chen,[†,‡] Kelong Ai,[†] Yanlan Liu,[†,‡] and Lehui Lu*[,†]

[†]State Key Laboratory of Electroanalytical Chemistry Changchun Institute of Applied Chemistry, Chinese Academy of Sciences, 5625 Renmin Street, Changchun 130022, P. R. China

[‡]University of the Chinese Academy of Sciences, Beijing 100039, China

Supporting Information

ABSTRACT: Imaging labels, therapeutic drugs, as well as many other agents can all be integrated into one nanoplatform to allow for molecular imaging and therapy. With this in mind, herein we report the first example of a tailor-made charge-conversional nanocomposite composed of mesoporous γ-AlO(OH) and upconversion nanoparticles (UCNPs) via a simple and versatile method, and the obtained nanocomposite could be performed as a drug delivery carrier and applied for cell imaging. The nanocomposite (UCNPs-Al) was found to be able to efficiently transport DOX, a typical chemotherapeutic anticancer drug, into the cancer cell and release DOX from UCNPs-Al triggering by the mildly acidic environment. In vitro cell cytotoxicity assay verified that DOX-loaded nanocomposites (UCNPs-Al-DOX) exhibited greater cytotoxicity with respect to free DOX at the same concentrations, because of the increase in cell uptake of anti-cancer drug delivery vehicles mediated by the charge-conversional property. Moreover, the UCL emission from UCNPs and the red fluorescence of DOX allow the nanocomposite to track and monitor the drug delivery system simultaneously. These findings have opened up new insights into designing and producing the highly versatile multifunctional nanoparticles for simultaneous imaging and therapeutic applications.

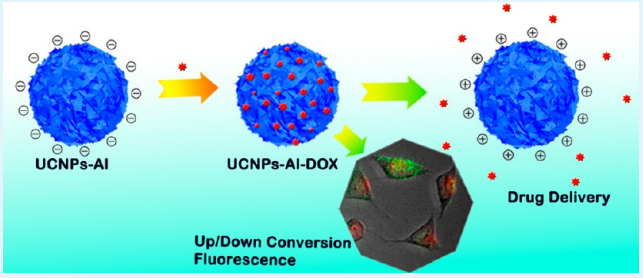

KEYWORDS: *upconversion, pH-responsive, charge-conversional, drug delivery, cell imaging*

1. INTRODUCTION

In the last two decades, a myriad of nanoparticle-based therapeutic and diagnostic agents have been developed for the treatment of various diseases. The use of materials in nanoscale provides unparallel advantages in many aspects of drug delivery.[1] Upconversion nanoparticles (UCNPs) have been widely investigated in multimodal imaging, photodynamic therapy (PDT), and photothermal therapy.[2−6] UCNPs utilize near-infrared excitation rather than ultraviolet excitation, and have unique properties including increasing the penetration depth in biological samples, minimizing background autofluorescence, photobleaching, and photodamaging biological specimens.[7−9] These fascinating optical features of UCNPs, as well as their small physical dimensions and biocompatibility, could enhance their prospects in the fields of imaging and therapy.[10−13]

From the viewpoint of practical applications, an ideal anticancer drug delivery system (DDS) should provide a sustained release in a controlled manner.[14] To achieve the goal, it is necessary to make the vehicle capable of storing and releasing therapeutic agents on command in response to external stimuli, such as pH, light and the temperature.[15−17] Of the stimuli previously studied, pH-responsiveness has shown great advantages and been frequently used in cancer therapy, as the tumor extracellular environment is more acidic than blood and normal tissues, and the pH values of endosome and lysosome are even lower.[18,19] However, the general strategy used in the drug delivery is based on the integration of UCNPs with mesoporous silica.[20,21] The porous silica layers endow the UCNPs with drug loading capability because of their porous structures. However, the conventional procedures usually require the intermediate coatings of solid silica and calcination process, thus leading to tedious multistep operations and complicated post-treatments. Furthermore, silica itself does not have any stimuli-responsive properties, unless it is decorated with some other functional materials.[17,22] As a result, it has been still a big challenge to develop new UCNPs-based nanocomposites for drug delivery, which has motivated us to design a new drug carrier with simple operations that could respond to pH variations for controlled release.

Besides controlling, the DDS always requires the delivery vehicle to accumulate within a target zone and release drug effectively. Many strategies have been proposed to target nanomaterials to certain antigens and receptor, which is aberrantly up-regulated on the surface of cancer cells. And these methods typically involve the modification of nanoparticles with various targeting agents, such as proteins, antibodies and other biomolecules.[23−25] Nevertheless, Salvati

Received: October 28, 2013
Accepted: December 5, 2013
Published: December 5, 2013

et al. have shown that the targeting ability of such functionalized nanoparticles may disappear when placed in a biological environment.[26] Recently, Xu et al. have developed a targeted charge-reversal nanoparticle for drug delivery, which exhibited the improved efficiency against cancer cells.[27] However, hitherto, most charge-conversional drug conjugates are based on block polymers.[28,29] Although the pH-sensitive polymers showed the ability of escape from the lysosomes and traverse into the nucleus, their applications are seriously limited by complicated preparations and safety concerns. Considering the advantages over polymers with simple operations and noninvolvement of toxic reagents, inorganic materials might be good candidates for constructing the targeted charge-conversional nanocomposites. To the best of our knowledge, the targeted charge-conversional drug delivery system integrated with UCNPs has not been reported yet.

Building from the above ideas, we introduced a cheap and low-toxicity inorganic nanomaterial, γ-AlO(OH) (boehmite), which has shown great potential for applications in biomedicine.[30−32] Until now, There are many literatures reports on aluminum-based inorganic nanomaterials, which have been applied in drug delivery, adsorption, and bioimaging.[33−37] Aluminum in the form of aluminum hydroxide, aluminum phosphate or alum has been commonly used as an adjuvant in many vaccines licensed by the US Food and Drug Administration, because of its excellent safety record.[38] Additionly, alumina is a material that has been used in both dental and orthopedic applications, and even demonstrated increased osteoblast functions.[39,40] By means of fundamental materials science as well as by applicational aspects for biomedical purposes, however, non-agglomerated and nanoscale spheres with multifunctional properties are still requested. Here, we further proceeded to prepare a novel nanocomposite consisting of UCNPs and boehmite (denoted as UCNPs-Al) via a microemulsion-based approach. With the facile strategy, the as-prepared nanocomposites simultaneously possessed mesoporous structures and upconversion luminescence (UCL) property. Importantly, they were able to exhibit pH-responsive and charge-conversional behaviors, which could enhance the cellular uptake and success of chemotherapy, and serve as a probe to monitor drug delivery process by fluorescence imaging synchronously.

2. EXPERIMENTAL SECTION

2.1. Materials. The rare-earth oxides including yttrium oxide (Y_2O_3, >99.99%), ytterbium oxide (Yb_2O_3, >99.99%), and erbium oxide (Er_2O_3, >99.99%) were purchased from Changchun Hepalink rare-earth materials company. The Y_2O_3, Yb_2O_3, and Er_2O_3 were reacted with excess hydrochloric acid to form the rare earth chloride compounds, respectively. After the hydrochloric acid and water were evaporated, the resulting powders were re-dispersed in water to yield the YCl_3 (1.0M), $YbCl_3$ (0.5M), and $ErCl_3$ (0.1M) aqueous stocking solutions, separately. Oleic acid (OA, 90%), octadecene (ODE, 90%), polyoxyethylene (5) nonylphenyl ether (Igepal CO-520, average Mn = 441), ammonia solution (28.0-30.0% NH_3 by weight) ,and 3-(4, 5-dimethylthiazol-2-yl)-2, 5-diphenyltetrazolium bromide (MTT) were obtained from Sigma-Aldrich. Aluminium isopropoxide (purity≥99.5%) was purchased from Tianjin Guangfu Fine Chemical Research Institute. Doxorubicin hydrochloride (DOX) was purchased from Sangon (Shanghai, China). Dulbecco's modified Eagle's medium (DMEM) and fetal bovine serum (FBS) were purchased from Gibco (New York, USA). All chemicals were analytical grade and used as received without further purification. Water used in the experiment was purified by a Millipore system.

2.2. Synthesis of UCNPs. UCNPs were synthesized according to a previously reported method with slight modification. Typically, YCl_3 aqueous solution (1.17 mL, 1.0 M), $YbCl_3$ aqueous solution (0.6 mL, 0.5 M), and $ErCl_3$ aqueous solution (0.3 mL, 0.1 M) were injected in a 50 mL flask and dried by heating. Then, oleic acid (9 mL) and octadecene (23 mL) were added into the flask. The solution was heated to 160 °C under argon protection to yield a homogeneous solution, and then cooled to room temperature. Subsequently, methanol solution (15 mL) containing NH_4F (0.222 g, 6 mmol) and NaOH (0.15 g, 3.75 mmol) was slowly added into the mixture. After vigorous stirring for 30 min, the solution was slowly heated to 220 °C to remove the residual water and impurities with low boiling point, and then heated to 310 °C and maintained for 1 h under argon protection. After cooling to room temperature naturally, the nanoparticles were collected by centrifugation (10 000 rpm for 10 min) and washed three times with ethanol. Finally, the nanoparticles were redispersed in cyclohexane.

2.3. Synthesis of UCNPs-Al. In brief, UCNPs in cyclohexane solution (2 mL, 17 mg mL^{-1}) and Igepal CO-520 (0.6 mL) were added in cyclohexane (38 mL) followed by ultrasonic treatment for 20 min. Then Igepal CO-520 (2.8 mL) was added. The resulting solution was vigorously stirred at room temperature for 3 h. Subsequently, ammonia solution (0.544 mL) was added under stirring. A few minutes later, aluminium isopropoxide (0.0741 g, dispersed in cyclohexane and methylbenzene with the volume ratio of 1:1) was added into the transparent microemulsion slowly. The mixture was allowed to age for 24 h to hydrolysis and condensation of the aluminum precursor. The products were precipitated by adding diethylene glycol (DEG) to the micellar system, separated by centrifugation, and washed with ethanol. The content of ammonia solution and aluminium isopropoxide has been optimized (see Figure S6 in the Supporting Information). Mesoporous silica-coated UCNPs (UCNPs-mSiO_2) were prepared as previously reported[41] (see Figure S9 in the Supporting Information).

2.4. DOX Loading and Release in Vitro. DOX loading onto UCNPs-Al was done by mixing DOX (4 mL, 1 mg mL^{-1}) with UCNPs-Al (2 mL, 5 mg mL^{-1}) in nanopure water, followed by shaking for 24 h in the dark at room temperature. The unbound excess DOX was removed by washing the products thoroughly with water to obtain the drug-loaded UCNPs-Al (UCNPs-Al-DOX), and the centrifugation speed used in the experiment was 10 000 rpm for 15 min (see Figure S8a in the Supporting Information). The DOX loading was calculated from the difference in concentrations of the initial and left, which was determined to be 0.02 mmol g^{-1} approximately.

For DOX release, UCNPs-Al-DOX was sealed in a dialysis bag (molecular weight cutoff = 8000) and immersed in 5 mL of buffer solution with different pH values at 37 °C with gentle shaking. At predetermined time intervals, the released DOX in the buffer was collected and replaced with an equal volume of fresh solution. In addition, the amounts of released DOX in the supernatant solutions were determined by monitoring the changes of the absorbance peak at 480 nm. The loading and release processes for UCNPs-mSiO_2 were the same as above.

2.5. Confocal Laser Scanning Microscopy (CLSM). The HeLa cells were incubated in 5% CO_2 atmosphere at 37 °C for 24 h, and then treated with UCNPs-Al-DOX at different concentrations. After incubated for 5 h, the cells were washed with PBS (pH 7.4) three times before analysis to remove free nanocomposites and transferred to fresh culture medium. As a control, the HeLa cells with blank and incubated with UCNPs-Al were also carried out. All images were collected by CLSM under the same instrumental conditions.

2.6. UCL Imaging and Measurement. The HeLa cells were seeded in 6-well culture plates. After grown in fresh medium in 5% CO_2 atmosphere at 37 °C for 24 h, the cells were incubated with UCNPs-Al or UCNPs-Al-DOX for a specific time. Thereafter, the cells were washed with PBS three times and imaged by a reconstructive Nikon Ti−S fluorescent microscope equipped with a NIR laser at 980 nm (BWT Beijing Ltd., China). The emissions from UCNPs-Al (green colored) and DOX fluorescence (red colored) were collected by the

excitation of 980 and 488 nm, respectively. All images were taken under the same instrumental conditions.

2.7. Flow Cytometry. The HeLa cells (1×10^5) were seeded in 6-well culture plates and cultured for 48 h. The cells were then treated with UCNPs-Al-DOX or free DOX ([DOX] = 20 μg mL^{-1}) at 37 °C for 4 h. A single cell suspension was prepared consecutively by trypsinization, washing with PBS, and then the suspended cells were filtrated, lifted using a cell stripper (Media Tech. Inc.), and analyzed using a FACS-Calibur flow cytometer (BD Biosciences) for DOX. All the cells were determined from a fluorescence scan performed with 1×10^4 cells.

2.8. Cytotoxicity Assays. To evaluate the cytotoxicity of UCNPs-Al, the MTT assay was used on the HeLa cell. Briefly, HeLa cells were seeded in a 96-well plates at a density of 6000−7000 cells per well, cultured with fresh DMEM, and supplemented with 20 % FBS under a humidified 5% CO_2 at 37 °C for 24 h. After that, various concentrations of UCNPs-Al, UCNPs-Al-DOX, and free DOX were added into the culture wells and the cells were further incubated for 24 h or 48 h. Subsequently, the cells were washed with culturing medium and treated with 10 μL MTT (5 mg mL^{-1} in PBS) at 37 °C for 4 h in an incubator at the same conditions. Finally, the supernatant was removed, and dimethyl sulfoxide (DMSO) was added (100 μL per well) and shaken for 10 min to thoroughly mix the formazan into the solvent. The optical density at 555 nm was measured by the microtiter plate reader. The untreated HeLa cells were used as control samples. The percentages of cell viabilities were calculated by using the optical densities with respect to the control values.

2.9. Hemolysis Assay in Vitro. Human blood samples stabilized by heparin were obtained from the local hospital. First, 1 mL of blood sample was added to 2 mL of PBS, and then red blood cells were isolated from serum by centrifugation. After being washed several times with PBS solution, the purified blood was diluted with PBS. Second, 0.2 mL of diluteded blood cells suspension was mixed with (a) 0.8 mL of PBS as a negative control, (b) 0.8 mL of water as a positive control, (c) 0.8 mL of UCNPs-Al suspensions at concentrations ranging from 12.5 to 1000 μg mL^{-1}. And then all the mixtures were vortexed and kept at room temperature for 3 h. Finally, the mixtures were centrifuged, and the absorbance of supernatants at 541 nm was determined by UV−vis spectra. The hemolysis percent of the red blood cells was calculated as following: Hemolysis Percentage = [(sample absorbance − negative control absorbance)/(positive control absorbance − negative control absorbance)] × 100.

3. RESULTS AND DISCUSSION

3.1. Synthesis and Characterization of UCNPs-Al. Yb and Er co-doped $NaYF_4$ nanoparticles (Y:Yb:Er = 78%:20%:2%) stabilized with oleic acid (OA) were synthesized by a modified solvothermal route. The UCNPs were well-dispersed in a nonpolar solvent (e.g., cyclohexane, chloroform, dichloromethane) without any detectable agglomeration. The TEM images showed that the particles had uniform size and shape, and the average diameters of UCNPs were measured to be approximately 33 nm (Figure 1b). The XRD diffraction peaks could be indexed to pure hexagonal-phase $NaYF_4$ crystals (JCPDS No.28-1192) (see Figure S3a in the Supporting Information). The high-resolution TEM image in the inset of Figure 1b revealed the lattice fringes with an observed *d*-spacing of 0.29 nm, corresponding to the lattice spacing in the (101) phases of the hexagonal $NaYF_4$ crystalline structures. Nevertheless, with the hydrophobic oleate capping ligand, the as-prepared UCNPs have no intrinsic aqueous solubility. Therefore, surface functionalization with hydrophilic materials is required prior to the biomedical applications.

As illustrated by Figure 1a, the UCNPs-Al were realized via the reverse microemulsion method, by using Igepal CO-520 as a surfactant, aluminium isopropoxide as an aluminium source, and simultaneously applying the liquid-to-liquid-phase boundary of the micellar system as a template. The morphology of the as-synthesized UCNPs-Al was characterized by TEM (Figure 1c) and SEM (Figure 2b). It can be revealed that the UCNPs-Al possessed a roughly spherical shape and well-defined layered structures. Energy-dispersive X-ray spectroscopy (EDS) (see Figure S1 in the Supporting Information) and X-ray photoelectron spectroscopy (XPS) spectra (see Figure S2 in the Supporting Information) manifested the existence of aluminum. Moreover, the binding energy of Al (2p, 73.6 eV) and O (1s, 533.0 eV, 531.7 eV, 530.7 eV) corresponded well with the presence of γ-AlO(OH).[42] As depicted in Figure S3b in the Supporting Information, a broad peak centered at 2θ = 14° can be observed because of the characteristic diffraction from γ-AlO(OH) (JCPDS No. 21-1307, (020) lattice plane), the other sharp peaks were in good agreement with those of hexagonal-phase $NaYF_4$ crystals, and it indicated that there was no phase transformation of $NaYF_4$ occurred in the process. However, the thin crystalline shell might have led to the comparably weak diffraction signal of γ-AlO(OH).

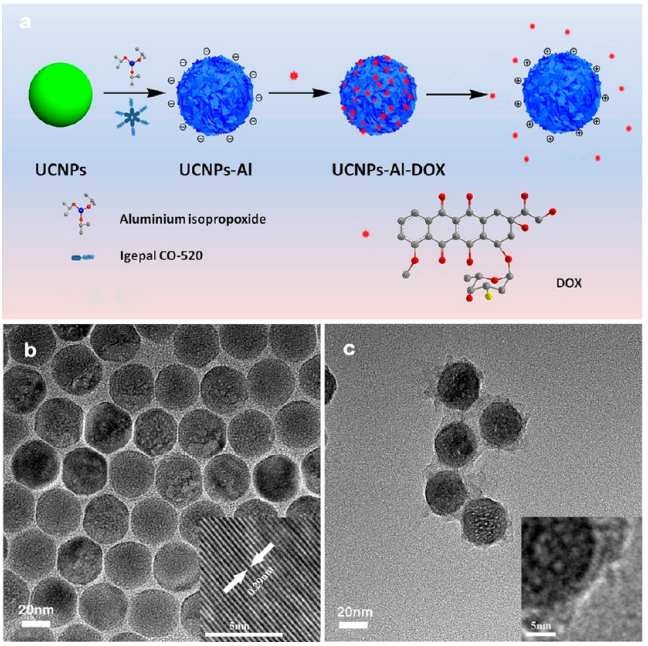

Figure 1. (a) Schematic representation for the synthesis of UCNPs-Al and the pH-responsive drug delivery process.TEM and high-resolution TEM micrographs of (b) UCNPs and (c) UCNPs-Al.

To further confirm the change of the surface structure, FTIR spectroscopy measurement was conducted (see Figure S4 in the Supporting Information). The UCNPs exhibited the characteristic peaks of oleic acid (OA) molecules. Absorbing bands at 2928 cm^{-1} and 2854 cm^{-1} were assigned to the asymmetric and symmetric stretching vibrations of $-CH_2$, respectively. Additionally, two peaks centered at 1564 cm^{-1} and 1465 cm^{-1} corresponded to asymmetric and symmetric stretching vibrations of carboxylic group (COO^-) of OA, respectively.[11] As-obtained UCNPs-Al, the stretching vibrations of CH_2 have been vanished with the appearance of new bands located at 1160 cm^{-1} (δ_s Al−O−H), 1070 cm^{-1} (δ_{as} Al−O−H) and 2080 cm^{-1} (combination bands), whereas other strong bands of OH (3468 cm^{-1}, 3550 cm^{-1}), and H_2O (1630 cm^{-1}) were also observed.[43] The results further revealed that the surface packing of UCNPs with γ-AlO(OH) was successful. The amount of γ-AlO(OH) was determined to be approx-

dx.doi.org/10.1021/am404761h | ACS Appl. Mater. Interfaces 2014, 6, 655−663

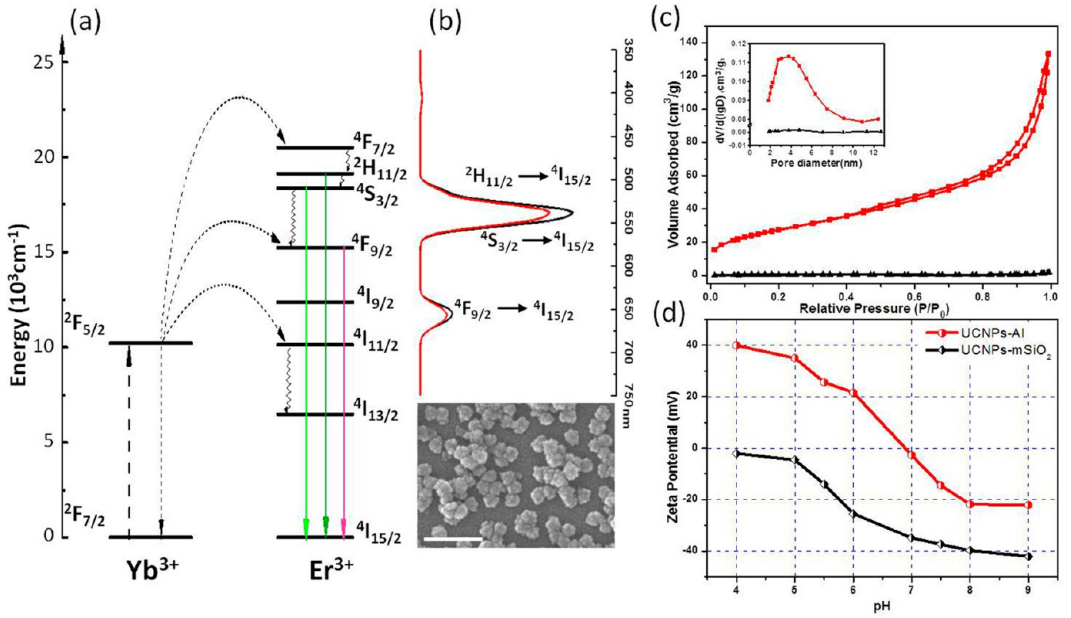

Figure 2. (a) Upconversion luminescence mechanism of UCNPs (λ_{ex} = 980 nm). (b) UCL spectra of as-synthesized UCNPs (black line) and UCNPs-Al (red line) under the same concentration ([*Y*] = 50 μg mL^{-1}); inset shows the SEM image of UCNPs-Al, the scale bar is 200 nm. (c) Nitrogen adsorption−desorption isotherms and pore size distribution curves (inset) of the as-prepared UCNPs (black line) and UCNPs-Al (red line). (d) Zeta potential of UCNPs-Al and UCNPs-mSiO$_2$ as a function of pH values.

imately 12 % according to TGA results (see Figure S5 in the Supporting Information). The resulting UCNPs-Al was well-dispersed in water, normal saline solution, and fetal bovine serum (FBS), and these colloidal solutions can be stable for weeks (see Figure S7 in the Supporting Information). Moreover, after loading DOX (denoted as UCNPs-Al-DOX), the high solubility and stability of the nanocomposite has been maintained (see Figure S8b in the Supporting Information).

The typical upconversion emission mechanism for UCNPs is illustrated in Figure 2a. As a sensitizer, the $^2F_{7/2}$−$^2F_{5/2}$ transition of Yb^{3+} is well resonant with f-f transitions of Er^{3+}, thus facilitating efficient energy transfer from Yb^{3+} to Er^{3+}. Under a 980 nm laser excitation, the electron is excited from $^2F_{7/2}$ to $^2F_{5/2}$ of Yb^{3+}. After that, some energy is transferred back to the ground state, whereas other energy is simultaneously nonradiatively transferred to Er^{3+}. Subsequently, radiant transitions from the Er^{3+} energy levels result in the emissions at 520 nm ($^2H_{11/2}$−$^4I_{15/2}$), 540 nm ($^4S_{3/2}$−$^4I_{15/2}$) and 655 nm ($^4F_{9/2}$−$^4I_{15/2}$). Compared with the UCL spectrum of UCNPs, the UCNPs-Al have showed similar peak positions, but with a little decreased intensity (Figure 2b).

The nitrogen adsorption−desorption measurement was used to investigate the porosity of the samples. As shown in Figure 2c, UCNPs presented non-porous characteristics with a Brunauer−Emmett−Teller (BET) surface area of only 1.93 m^2 g^{-1}. On the contrary, UCNPs-Al exhibited the classical type-IV adsorption-desorption isotherms of mesoporous materials with BET surface area of 99.13 m^2 g^{-1}. Furthermore, UCNPs-Al had mesopores around 3−4 nm and a pore volume of 0.21 cm^3 g^{-1}, which would be enough for UCNPs-Al to load the adequate quantity of drugs when used as a drug delivery carrier.

Prior to using UCNPs-Al for intracellular drug delivery and imaging, their cytotoxicity was assessed by MTT assay. This crucial factor must be established in determining the suitability of UCNPs-Al for clinical applications. The HeLa cells were incubated with the UCNPs-Al in various concentrations for 24 h (see Figure S10 in the Supporting Information). Encouragingly, the cell viability was not hindered by UCNPs-Al up to a concentration of 100 μg mL^{-1}. Furthermore, the cell viability was still about 100 % even prolonging the time of incubation to 48 h (Figure 6), thereby revealing the remarkably low cytotoxicity of UCNPs-Al. The hemolysis assay experiments were carried out as an important factor to evaluate the biocompatibility. The hemolytic assay (see Figure S11 in the Supporting Information) demonstrated that nearly no hemolysis of red blood cells could be detected upon the maximal experimental concentration (1000 μg mL^{-1}), indicating their admirable blood compatibility for the further in vivo therapeutic investigation.

3.2. Drug Loading and Releasing. To demonstrate the potential applications of UCNPs-Al, we have investigated the change of zeta potential values at different pH (Figure 2d). It is noted that the UCNPs-Al have shown charge-conversional behavior from weakly alkaline to acidic medium. The increasing acidity resulted in a constant increase in the positive charge of the nanocomposite, thus endowing the nanocomposite with the ability to change the zeta potential according to the environmental pH. This phenomenon may be attributed to the protonation/deprotonation of the hydroxyl groups on the surface of the nanocomposite, since the isoelectric point of UCNPs-Al is approximately 6.9.[44] Moreover, UCNPs-Al revealed a zeta potential of about −17 mV at pH 7.4, and remained negative for 60 min. When the pH of the solution changed to 5.0, they immediately became positively charged as high as +38 mV for another 60 min (see Figure S12 in the Supporting Information). Thus, UCNPs-Al were negatively charged at physiological pH, and converted to positive at lower pH. By contrast, the UCNPs-mSiO$_2$ were almost negatively charged over the wide pH range from 4.0 to 9.0 (Figure 2d). Recently, Kim et al. have indicated that the positive-charged particles may be more effective for drug delivery, because they are taken up to a greater extent by proliferating cells.[45] In this

dx.doi.org/10.1021/am404761h | ACS Appl. Mater. Interfaces 2014, 6, 655−663

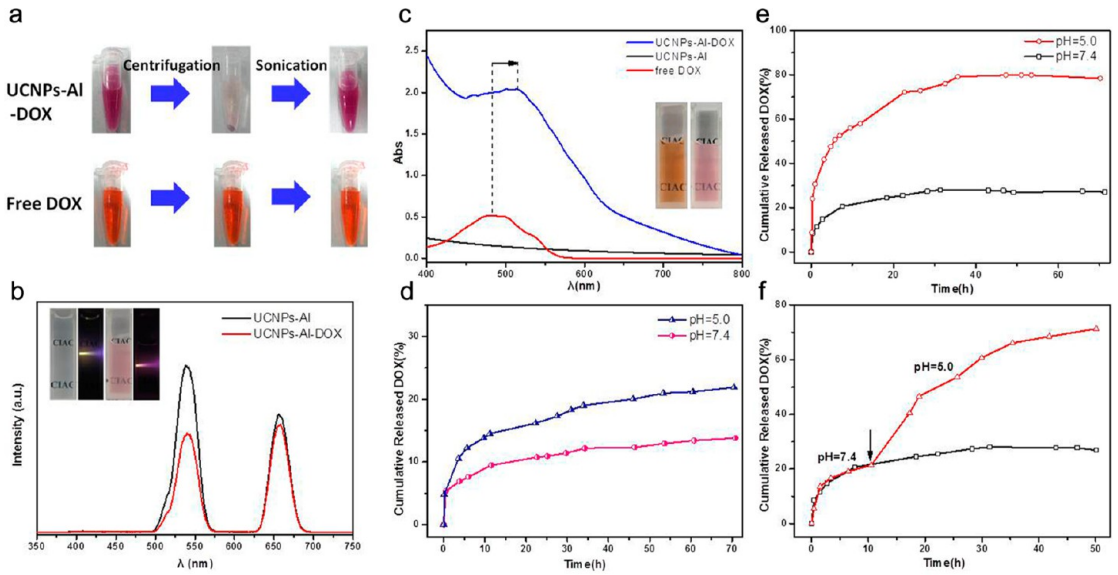

Figure 3. (a) Pictures of UCNPs-Al-DOX and free DOX after centrifugation and then sonication. (b) UCL spectra of UCNPs-Al and UCNPs-Al-DOX aqueous solution at the same concentration of 0.5 mg mL^{-1}; inset is photos of UCNPs-Al (left side) and UCNPs-Al-DOX (right side) under the ambient light and the excitation by a 980 nm laser in the dark, respectively. (c) UV−vis spectra of UCNPs-Al-DOX, UCNPs-Al and free DOX, the inset photographs were free DOX (left) and UCNPs-Al-DOX (right). (d) Cumulative release curves of DOX from UCNPs-$mSiO_2$. (e) Releasing profile of DOX from UCNPs-Al-DOX at different pH and (f) delayed release of DOX from the nanocomposite when the pH value is changed from 7.4 to 5.0 after incubation for 11 h.

case, the charge-conversional property of UCNPs-Al will be expected to enhance their internalization at mildly acidic environment.

As discussed above, the as-prepared UCNPs-Al not only possessed charge-conversional property, but also had mesoporous nanostructures, all of which have played key roles in the absorbing and releasing process of drugs. DOX, a typical chemotherapeutic anticancer drug, was introduced into UCNPs-Al. The zeta potential of UCNPs-Al-DOX was about −12 mV at pH 7.4, and a slight increase was observed compared to the UCNPs-Al carrier. This phenomenon could be attributed to the successful loading of DOX, which was positively charged.[46,47] Moreover, compared with UCNPs-Al, the diameter of UCNPs-Al-DOX kept around 45 nm, and the morphology of the nanocarrier was scarcely changed after loading DOX (see Figure S13 in the Supporting Information). During the drug-loading process, free DOX and UCNPs-Al were mixed together and shaken for 24 h in the dark. Because of a positively charged nature of aromatic molecule, DOX would interact electrostatically with UCNPs-Al at physiological pH, because the UCNPs-Al was negatively charged under such condition. After that, the DOX-loaded sample was collected by centrifugation, until there was no visible color in the supernatant. Upon sonicating for a while, the precipitate was completely re-dispersed in water with a pink color (Figure 3a). In contrast, free DOX remained a transparent solution with an orange color. These photographs implied that DOX has been successfully loaded on the UCNPs-Al. Figure 3c compared the UV−vis spectra of free DOX and UCNPs-Al-DOX. It is evident that DOX loading on UCNPs-Al caused a red shift from 480 nm to 515 nm, well-consistent with the color change from orange to pink. Accordingly, the UCL spectra of UCNPs-Al-DOX have showed a decreased ratio of green to red emission, because of the fact that the DOX mainly quench the emission band from 500 nm to 560 nm (Figure 3b). The red shift suggested that the drug should have been coordinated with aluminum. It is commonly accepted that aluminum is able to coordinate with various organic ligands, which would form the well-known Al-based porous coordination polymer (Al-PCP).[48] However, the formation and breakage of the coordination-bonding architectures are sensitive to external pH variations, and such properties has been used for the pH-responsive drug delivery.[49] On the other hand, it was previously reported that the drug was able to form a coordinate bond with metal ions, which demonstrated an improved therapeutic profile.[50] Nevertheless, the therapeutic efficiency of UCNPs-Al-DOX will be verified later.

Along with reducing the pH value, UCNPs-Al became positive charged. At the same time, the force between the nanocomposite and DOX got repulsive, and then the burst release of DOX has been achieved. The cumulative drug releasing profile of UCNPs-Al-DOX has showed pH-dependent properties (Figure 3e). In the normal physiological conditions (pH 7.4), about 27% of DOX was released within 30 h. Upon changing the pH value to 5.0, the total released amount of DOX was three-fold larger than that at pH 7.4 in the same situation. To validate the efficiency of the pH-triggered controllable cargo releasing process with UCNPs-Al, we carried out the release system at pH 7.4 in the first eleven hours. By adjusting the pH value to 5.0 with the addition of HCl solution, we accomplished the activation of drug release from the nanocomposite (Figure 3f). One can ascribe the results to the fact that DOX has increased hydrophilicity and solubility at lower pH, which is caused by the enhanced protonation of the $-NH_2$ group of DOX,[51,52] and consequently DOX was pumped out by repulsion of the positive-charged UCNPs-Al. In the control experiment, UCNPs-$mSiO_2$ as a drug delivery carrier was also investigated and revealed that about 13 % of DOX was released at pH 7.4. Even at pH 5.0, the released DOX was found to be merely 21% (Figure 3d). Obviously, compared to the UCNPs-Al drug delivery system, UCNPs-$mSiO_2$ failed to release DOX completely, and its pH-responsive drug release

dx.doi.org/10.1021/am404761h | ACS Appl. Mater. Interfaces 2014, 6, 655−663

behavior depended strongly on the properties of DOX itself.[53] The above results revealed that UCNPs-Al as the pH-responsive drug delivery system would offer a desirable way for specific target and controllable release.

3.3. Intracellular Drug Delivery and Imaging. As mentioned above, the nanocomposite possessed unique characters of weak auto-fluorescence background, greater tissue penetration, and excellent chemical stability, all of which have made the nanocomposite a promising candidate for biological imaging. The UCL imaging of UCNPs-Al was performed to testify the cellular uptake process of the nanocomposite. The HeLa cells were incubated with UCNPs-Al for different period of time at 37 °C and washed with fresh PBS prior to the fluorescence imaging. As seen from the images in Figure 4, the

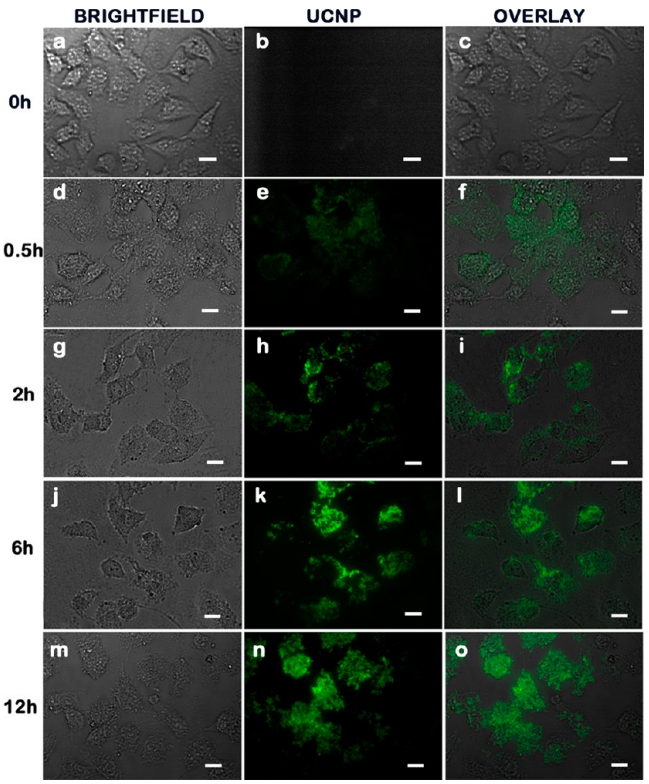

Figure 4. UCL images of HeLa cells incubated with UCNPs-Al (200 μg mL^{-1}) for 0, 0.5, 2, 6, and 12 h under 980 nm laser excitation. (a, d, g, j, m) Bright-field images, (b, e, h, k, n) UCL images in dark-field, and (c, f, i, l, o) the emerged images of the corresponding cells after incubation. All scale bars are 20 μm.

UCL intensity of stained HeLa cells increased dramatically as prolonging the incubation time to 12 h. The HeLa cells incubated throughout the imaging experiments were viable, which was evidenced by the bright-field images. The results indicated that a growing number of nanocomposites were taken up by HeLa cells, and the nanocomposite could be served as a novel agent for optical imaging.

To investigate intracellular release behavior of UCNPs-Al-DOX, we applied the confocal laser scanning microscopy (CLSM), which demonstrated the red fluorescence of DOX upon the excitation at 488 nm (see Figure S14 in the Supporting Information). Different concentrations of UCNPs-Al-DOX were incubated with HeLa cells for a 5.0 h period. It showed that the fluorescence intensity of stained HeLa cells increased with increasing the concentration of UCNPs-Al-DOX. The results can be attributed to the fact that the detachment of DOX from the nanocomposite was achieved after endocytosis, which was triggered by the endosomes or lysosomes with lower pH. The HeLa cells as a control and incubated with pure UCNPs-Al had no fluorescence under the same situation. These images have shown a concentration-dependent internalization process that the DOX molecules were gradually released from the nanocomposite with a high efficiency.

Moreover, using a modified fluorescent microscope with an external 980 nm laser as the excitation source, upconversion signals, as well as downconversion fluorescence of DOX, can be obtained simultaneously (Figure 5). After incubated with the

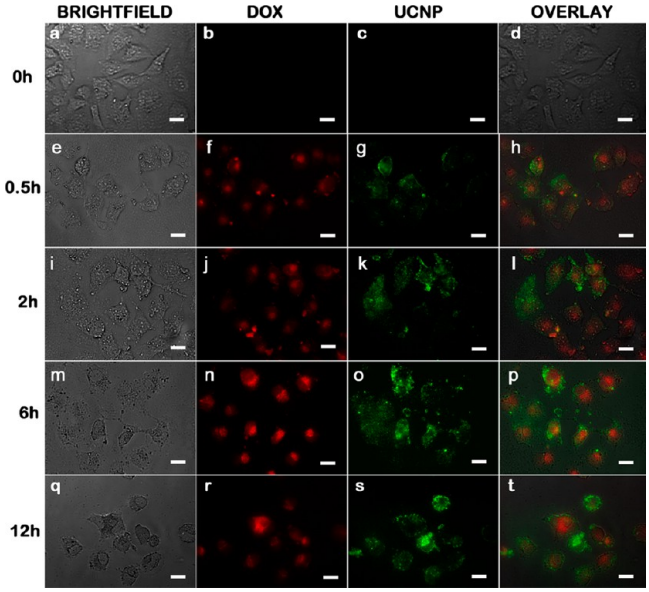

Figure 5. Microscopic imaging of HeLa cells after incubated with UCNPs-Al-DOX ([DOX] = 20 μg mL^{-1}) for 0, 0.5, 2, 6, and 12 h at 37 °C. (a, e, i, m, q) Bright-field images, (d, h, l, p, t) the emerged images of the corresponding cells after incubation. (b, f, j, n, r) DOX fluorescence (red colored) and (c, g, k, o, s) UCL emission (green colored) from UCNPs-Al-DOX were recorded under the excitation of 488 and 980 nm, respectively. All scale bars are 20 μm.

UCNPs-Al-DOX for 0 h, 30 min, 2 h, 6 h and 12 h at 37 °C, the HeLa cells showed highly distributed red fluorescence of DOX with growing intensity, suggesting the intracelluar release of DOX molecules from UCNPs-Al and the DOX was released in a slow and sustained way. Overlay of these images further demonstrated that both UCL luminescence and the DOX red fluorescence were evident in the whole intracellular region, which was in agreement with the CLSM images. These experiments further confirmed that after passing through the cytomembrane, the nanocomposite would release DOX molecules triggered by the endosomes or lysosomes with lower pH, which eventually penetrated into the nuclei to kill the cells.

3.4. Cytotoxicity of UCNPs-Al-DOX. Following cellular internalization, the key issue is whether DOX was efficiently released to kill the cancer cells. To evaluate the therapeutic efficiency of the nanocomposite, the cytotoxic effect of UCNPs-Al-DOX on HeLa cells was assessed by MTT assay and the results were compared with free DOX and UCNPs-Al (Figure 6). In the absence of drug, pure UCNPs-Al had negligible effects on cell viability. Meanwhile, DOX alone exhibited dose-

dx.doi.org/10.1021/am404761h | ACS Appl. Mater. Interfaces 2014, 6, 655−663

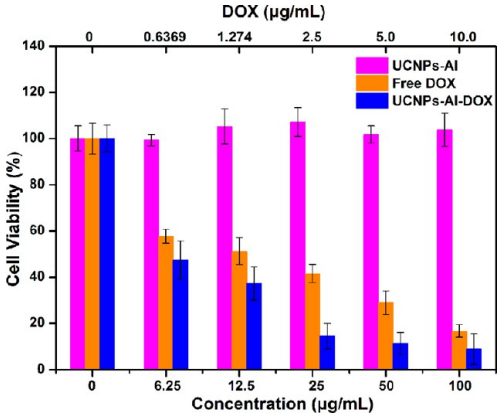

Figure 6. Viability of HeLa cells in the presence of UCNPs-Al, free DOX, and UCNPs-Al-DOX with varied concentrations.

dependent inhibition against HeLa cells. The half-maximal inhibitory concentration (IC_{50}) of free DOX was estimated to be about 1.42 μg mL^{-1}. The UCNPs-Al-DOX showed similar inhibition effect against HeLa cells with an estimated IC_{50} of 0.6 μg mL^{-1}, which implied significantly more toxic in reducing viability of HeLa cells than free DOX. Because the mechanism of chemotherapy requires DOX to enter into the nucleus, it suggested that the DOX should be efficiently released from the nanocomposite after cell internalization.[54] Moreover, one can speculate that the DOX encapsulated in the nanocomposite can be protected from the drug degradation by intracellular enzymes and environment during delivery and therefore preserves its anticancer activity.[55]

To investigate the mechanism of the higher cytotoxicity induced by DOX loaded UCNPs-Al, we demonstrated the flow cytometry analysis, and used it to quantitatively evaluate the cellular association of UCNPs-Al-DOX in a cell line (Figure 7). The cell uptake degree of the nanocomposite could be quantified by determining the red fluorescence emitted from the released DOX. After incubating for 4 h, the amount of red fluorescence from UCNPs-Al-DOX was much higher than that in the control cells, and even higher than the free DOX, which have indicated that the UCNPs-Al nanocomposite, as a drug carrier, enhanced the cellular uptake of DOX. Thus, we attributed the enhanced cytotoxicity of UCNPs-Al-DOX to the sustained release of drug and efficient cellular uptake caused by the charge-conversional property.[56,57]

4. CONCLUSIONS

In summary, a novel core/shell structured UCNPs-Al nanocomposite were designed and prepared for pH-responsive drug delivery and cell imaging via the reverse microemulsion method. These nanocomposites were found to be able to efficiently transport DOX into the cancer cell and release DOX from UCNPs-Al by adjusting the pH value. In comparison with previously reported nanocomposite-based DOX-release system, the UCNPs-Al had three advantages. Firstly, the preparation steps of the vehicle was quite simple. Secondly, the charge-conversional property has endowed the nanocomposite with enhanced cellular uptake and cytotoxicity to the cancer cells. Thirdly, the UCL emission from UCNPs and the red fluorescence of DOX allow the nanocomposite to track and monitor the drug delivery system simultaneously, and it would be helpful to disclose the whole mechanism of drug delivery. Moreover, both hemolysis and MTT assay confirmed the negligible toxicity and good biocompatibility of UCNPs-Al. These unique characters of UCNPs-Al would make the nanocomposite a practically applicable platform for further cancer therapy and imaging in vivo.

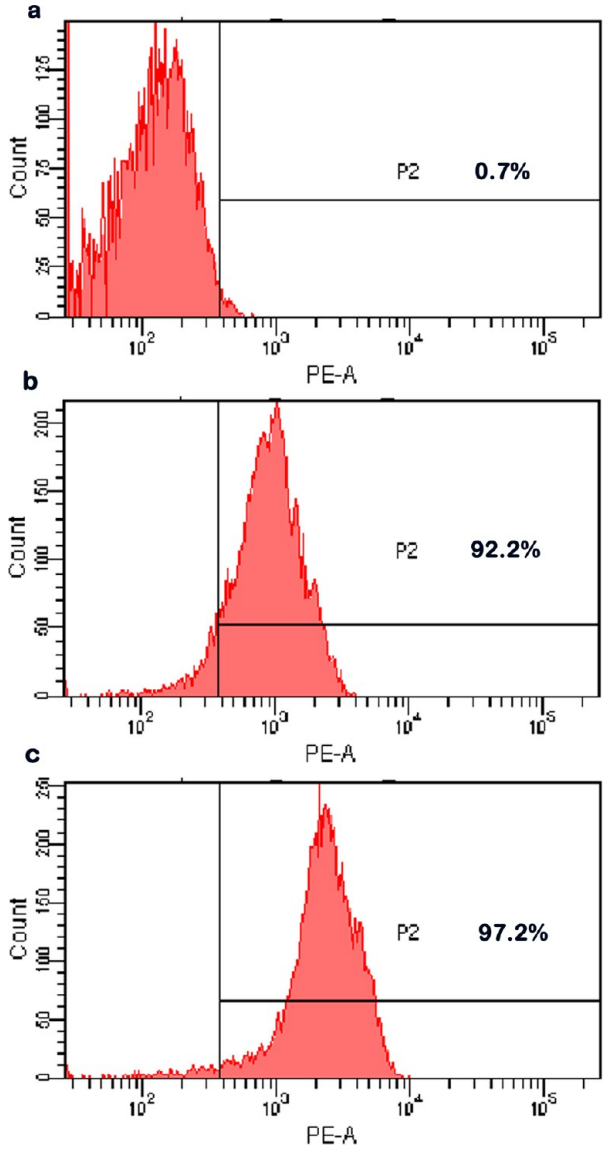

Figure 7. Flow cytometry analysis of (a) the control cells and HeLa cells incubated with (b) free DOX, (c) UCNPs-Al-DOX for 4 h.

■ ASSOCIATED CONTENT

Supporting Information

EDS, XPS, XRD, TGA, and FTIR spectra of UCNPs and UCNPs-Al; the optimized reaction conditions for UCNPs-Al; the photos of centrifugation and dispersion in various physiological medium; the TEM image of UCNPs-mSiO_2; the MTT and hemolysis assay of UCNPs-Al; the zeta potential data of UCNPs-Al at different pH; the TEM images of UCNPs-Al and UCNPs-Al-DOX; and the confocal fluorescence images of HeLa cells incubated with UCNPs-Al-DOX and UCNPs-Al, respectively. This material is available free of charge via the Internet at http://pubs.acs.org/.

dx.doi.org/10.1021/am404761h | ACS Appl. Mater. Interfaces 2014, 6, 655−663

AUTHOR INFORMATION

Corresponding Author

*E-mail: lehuilu@ciac.ac.cn.

Notes

The authors declare no competing financial interest.

ACKNOWLEDGMENTS

Financial support by NSFC (21125521, 21075117) and the National Basic Research Program of China (973 Program, 2010CB933600) is gratefully acknowledged.

REFERENCES

(1) Zhang, L.; Gu, F. X.; Chan, J. M.; Wang, A. Z.; Langer, R. S.; Farokhzad, O. C. *Clin. Pharmacol. Ther.* **2008**, *83*, 761−769.

(2) Liu, F. Y.; He, X. X.; Liu, L.; You, H. P.; Zhang, H. M.; Wang, Z. X. *Biomaterials* **2013**, *34*, 5218−5225.

(3) Zhang, G.; Liu, Y. L.; Yuan, Q. H.; Zong, C. H.; Liu, J. H.; Lu, L. H. *Nanoscale* **2011**, *3*, 4365−4371.

(4) Wang, C.; Cheng, L.; Liu, Y. M.; Wang, X. J.; Ma, X. X.; Deng, Z. Y.; Li, Y. G.; Liu, Z. *Adv. Funct. Mater.* **2013**, *23*, 3077−3086.

(5) Cheng, L.; Yang, K.; Li, Y. G.; Zeng, X.; Shao, M. W.; Lee, S. T.; Liu, Z. *Biomaterials* **2012**, *33*, 2215−2222.

(6) Challenor, M.; Gong, P. J.; Lorenser, D.; Fitzgerald, M.; Dunlop, S.; Sampson, D. D.; Iyer, K. S. *ACS Appl. Mater. Interfaces* **2013**, *5*, 7875−7880.

(7) Gu, Z. J.; Yan, L.; Tian, G.; Li, S. J.; Chai, Z. F.; Zhao, Y. L. *Adv. Mater.* **2013**, *25*, 3758−3779.

(8) Haase, M.; Schäfer, H. *Angew. Chem., Int. Ed.* **2011**, *50*, 5808−5829.

(9) Pichaandi, J.; Veggel, F. C. J. M. V.; Raudsepp, M. *ACS Appl. Mater. Interfaces* **2010**, *2*, 157−164.

(10) Liu, Y. L.; Ai, K. L.; Liu, J. H.; Yuan, Q. H.; He, Y. Y.; Lu, L. H. *Angew. Chem., Int. Ed.* **2011**, *50*, 1−7.

(11) Liu, Y. L.; Ai, K. L.; Lu, L. H. *Nanoscale* **2011**, *3*, 4804−4810.

(12) Cui, S. S.; Yin, D. Y.; Chen, Y. Q.; Di, Y. F.; Chen, H. Y.; Ma, Y. X.; Achilefu, S.; Gu, Y. Q. *ACS Nano* **2013**, *7*, 676−688.

(13) Shan, G. B.; Assaaoudi, H.; Demopoulos, G. P. *ACS Appl. Mater. Interfaces* **2011**, *3*, 3239−3243.

(14) Zhang, Z. Y.; Xu, Y. D.; Ma, Y. Y.; Qiu, L. L.; Wang, Y.; Kong, J. L.; Xiong, H. M. *Angew. Chem., Int. Ed.* **2013**, *52*, 1−6.

(15) Dai, Y. L.; Yang, D. M.; Ma, P. A.; Kang, X. J.; Zhang, X.; Li, C. X.; Hou, Z. Y.; Cheng, Z. Y.; Lin, J. *Biomaterials* **2012**, *33*, 8704−8713.

(16) Liu, J. N.; Bu, W. B.; Pan, L. M.; Shi, J. L. *Angew. Chem., Int. Ed.* **2013**, *52*, 4375−4379.

(17) Dai, Y. L.; Ma, P. A.; Cheng, Z. Y.; Kang, X. J.; Zhang, X.; Hou, Z. Y.; Li, C. X.; Yang, D. M.; Zhai, X. F.; Lin, J. *ACS Nano* **2012**, *6*, 3327−3338.

(18) Mellman, I.; Fuchs, R.; Helenius, A. *Annu. Rev. Biochem.* **1986**, *55*, 663−700.

(19) Tannock, I. F.; Rotin, D. *Cancer Res.* **1989**, *49*, 4373−4384.

(20) Qian, H. S.; Guo, H. C.; Ho, P. C.; Mahendran, R.; Zhang, Y. *Small* **2009**, *5*, 2285−2290.

(21) Kang, X. J.; Cheng, Z. Y.; Li, C. X.; Yang, D. M.; Shang, M. M.; Ma, P. A.; Li, G. G.; Liu, N.; Lin, J. *J. Phys. Chem. C* **2011**, *115*, 15801−15811.

(22) Zhang, X.; Yang, P. P.; Dai, Y. L.; Ma, P. A.; Li, X. J.; Cheng, Z. Y.; Hou, Z. Y.; Kang, X. J.; Li, C. X.; Lin, J. *Adv. Funct. Mater.* **2013**, *23*, 4067−4078.

(23) Wang, M.; Mi, C. C.; Wang, W. X.; Liu, C. H.; Wu, Y. F.; Xu, Z. R.; Mao, C. B.; Xu, S. K. *ACS Nano* **2009**, *3*, 1580−1586.

(24) Dai, Y. L.; Kang, X. J.; Yang, D. M.; Li, X. J.; Zhang, X.; Li, C. X.; Hou, Z. Y.; Cheng, Z. Y.; Ma, P. A.; Lin, J. *Adv. Healthcare Mater.* **2013**, *2*, 562−567.

(25) Liu, J. N.; Bu, W. B.; Pan, L. M.; Zhang, S. J.; Chen, F.; Zhou, L. P.; Zhao, K. L.; Peng, W. J.; Shi, J. L. *Biomaterials* **2012**, *33*, 7282−7290.

(26) Salvati, A.; Pitek, A. S.; Monopoli, M. P.; Prapainop, K.; Bombelli, F. B.; Hristov, D. R.; Kelly, P. M.; Åberg, C.; Mahon, E.; Dawson, K. A. *Nat. Nanotechnol.* **2013**, *8*, 137−143.

(27) Xu, P. S.; Kirk, E. A. V.; Zhan, Y. H.; Murdoch, W. J.; Radosz, M.; Shen, Y. Q. *Angew. Chem., Int. Ed.* **2007**, *46*, 4999−4902.

(28) Lee, Y.; Fukushima, S.; Bae, Y.; Hiki, S.; Ishii, T.; Kataoka, K. *J. Am. Chem. Soc.* **2007**, *129*, 5362−5363.

(29) Zhou, Z. X.; Shen, Y. Q.; Tang, J. B.; Jin, E. L.; Ma, X. P.; Sun, Q. H.; Zhang, B.; Krik, E. A. V.; Murdoch, W. J. *J. Mater. Chem.* **2011**, *21*, 19114−19123.

(30) Buchold, D. H. M.; Feldmann, C. *Nano Lett.* **2007**, *7*, 3489−3492.

(31) Wang, X. P.; Li, X.; Sogo, Y.; Ito, A. *RSC Adv.* **2013**, *3*, 8164−8167.

(32) Kapusetti, G.; Mishra, R. R.; Srivastava, S.; Misra, N.; Singh, V.; Roy, P.; Kumar, S. S.; Chakraborty, C.; Malikf, S.; Maiti, P. *J. Mater. Chem. B* **2013**, *1*, 2275−2288.

(33) Zheng, Y. Y.; Ji, S. F; Liu, H. F.; Li, M.; Yang, H. *Particuology* **2012**, *10*, 751−758.

(34) Tyner, K. M.; Schiffmanb, S. R.; Giannelis, E. P. *J. Controlled Release* **2004**, *95*, 501−514.

(35) Shao, M. F.; Ning, F. Y.; Zhao, J. W.; Wei, M.; Evans, D. G.; Duan, X. *J. Am. Chem. Soc.* **2012**, *134*, 1071−1077.

(36) Oh, J. M.; Choi, S. J.; Lee, G. E.; Han, S. H.; Choy, J. H. *Adv. Funct. Mater.* **2009**, *19*, 1617−1624.

(37) Miao, Y. E.; Wang, R. Y.; Chen, D.; Liu, Z. Y.; Liu, T. X. *ACS Appl. Mater. Interfaces* **2012**, *4*, 5353−5359.

(38) Baylor, N. W.; Egan, W.; Richman, P. *Vaccine* **2002**, *20*, S18−S23.

(39) Webster, T. J.; Hellenmeyer, E. L.; Price, R. L. *Biomaterials* **2005**, *26*, 953−960.

(40) Price, R. L.; Gutwein, L. G.; Kaledin, L.; Tepper, F.; Webster, T. J. *J. Biomed. Mater. Res., Part A* **2003**, *67*, 1284−1293.

(41) Zhang, L. Y.; Wang, T. T.; Yang, L.; Liu, C.; Wang, C. G.; Liu, H. Y.; Wang, Y. A.; Su, Z. M. *Chem.—Eur. J.* **2012**, *18*, 12512−12521.

(42) Kloprogge, J. T.; Duong, L. V.; Wood, B. J.; Frost, R. L. *J. Colloid Interface Sci.* **2006**, *296*, 572−576.

(43) Yang, J. X.; Ma, J. J.; Huang, Y. W. *Mater. Sci. Forum* **2011**, *694*, 28−32.

(44) Zhang, Y. X.; Yu, X. Y.; Jin, Z.; Jia, Y.; Xu, W. H.; Luo, T.; Zhu, B. J.; Liu, J. H.; Huang, X. J. *J. Mater. Chem.* **2011**, *21*, 16550−16557.

(45) Kim, B.; Han, G.; Toley, B. J.; Kim, C.; Rotello, V. M.; Forbes, N. S. *Nat. Nanotechnol.* **2010**, *5*, 465−472.

(46) Wang, F.; Liu, B. W.; Ip, A. C.; Liu, J. W. *Adv. Mater.* **2013**, *25*, 4087−4092.

(47) Park, J. H.; Gu, L.; Maltzahn, G. V.; Ruoslahti, E.; Bhatia, S. N.; Sailor, M. J. *Nat. Mater.* **2009**, *8*, 331−336.

(48) Comotti, A.; Bracco, S.; Sozzani, P.; Horike, S.; Matsuda, R.; Chen, J. X.; Takata, M.; Kubota, Y.; Kitagawa, S. *J. Am. Chem. Soc.* **2008**, *130*, 13664−13672.

(49) Xing, L.; Zheng, H. Q.; Che, S. A. *Chem.—Eur. J.* **2011**, *17*, 7271−7275.

(50) Kheirolomoom, A.; Mahakian, L. M.; Lai, C. Y.; Lindfors, H. A.; Seo, J. W.; Paoli, E. E.; Watson, K. D.; Haynam, E. M.; Ingham, E. S.; Xing, L.; et al. *Mol. Biopharm.* **2010**, *7*, 1948−1958.

(51) Peng, F.; Su, Y. Y.; Wei, X. P.; Lu, Y. M.; Zhou, Y. F.; Zhong, Y. L.; Lee, S. T.; He, Y. *Angew. Chem., Int. Ed.* **2012**, *51*, 1−6.

(52) Liu, Z.; Sun, X. M.; Nakayama-Ratchford, N.; Dai, H. J. *ACS Nano* **2007**, *1*, 50−56.

(53) Fritze, A.; Hens, F.; Kimpfler, A.; Schubert, R.; Peschka-Süss, R. *Biochim. Biophys. Acta* **2006**, *1758*, 1633−1640.

(54) Wang, F.; Pauletti, G. M.; Wang, J. T.; Zhang, J. M.; Ewing, R. C.; Wang, Y. L.; Shi, D. L. *Adv. Mater.* **2013**, *25*, 3485−3489.

(55) Chen, A. M.; Zhang, M.; Wei, D. G.; Stueber, D.; Taratula, O.; Minko, T.; He, H. X. *Small* **2009**, *5*, 2673−2677.

(56) Zhang, F.; Braun, G. B.; Pallaoro, A.; Zhang, Y. C.; Shi, Y. F.; Cui, D. X.; Moskovits, M.; Zhao, D. Y.; Stucky, G. D. *Nano Lett.* **2012**, *12*, 61−67.

(57) Wei, W.; Ma, G. H.; Hu, G.; Yu, D.; Mcleish, T.; Su, Z. G.; Shen, Z. Y. *J. Am. Chem. Soc.* **2008**, *130*, 15808−15810.